Ceramics International xxx (xxxx) xxx

Contents lists available at ScienceDirect

Ceramics International

journal homepage: www.elsevier.com/locate/ceramint

Atmospheric plasma spraying of ytterbium disilicate for abradable and environmental barrier coatings: A story of processing-microstructure relationships

A. Lynam [a], A. Rincon Romero [a], F. Xu [a], G.J. Brewster [b], G. Pattinson [b], T. Hussain [a,*]

[a] Faculty of Engineering, University of Nottingham, NG7 2RD, UK
[b] Rolls-Royce Plc, London, UK

ARTICLE INFO

Handling Editor: Dr P. Vincenzini

ABSTRACT

Environmental barrier coatings (EBCs) are required to protect SiC based composites in high temperature, steam containing combustion environments found in the latest generation of high efficiency gas turbine aeroengines. Ytterbium disilicate (YbDS) has shown promise as an environmental barrier coating, showing excellent phase stability at high temperatures and a coefficient of thermal expansion close to that of SiC however its performance is dependent on the conditions under which the coating was deposited. In this work, a parametric study was undertaken to demonstrate how processing parameters using a widely used Praxair SG-100 atmospheric plasma spraying (APS) torch affect the phase composition, microstructure and mechanical properties of ytterbium disilicate. Ytterbium disilicate coatings were deposited using 4 sets of spray parameters, varying the spray power from 12 to 24 kW. The phases present in these coatings were quantified using x-ray diffraction with Rietveld refinement, and the level of porosity was measured. Using this data, the relationship between processing parameters and phase composition and microstructure was examined. Using the optimum process parameter window determined in this work, abradable YbDS coatings were deposited using polyester feedstock additions as a pore forming phase. Two different polyester levels were added to create coatings with two different porosity levels.

1. Introduction

As performance and efficiency gains in gas turbines are constantly sought, the temperatures under which Ni-based superalloys must operate are approaching their limit. Thermal barrier coatings (TBCs) have allowed turbine inlet temperatures of ~1500 °C, improving thrust outputs, thermal efficiency and reducing harmful emissions [1]. Even with the use of TBCs, the in-service temperature such components are exposed to is now approaching the melting point of the Ni alloys, so it is clear that new material solutions must be sought. One such solution is using SiC/SiC ceramic matrix composites (CMCs). CMCs show excellent high temperature mechanical properties, have a temperature limit ~200 °C higher than Ni based superalloys and have a lower density than their metallic counterparts (improving thrust to weight ratios) [2]. Nevertheless, SiC/SiC CMCs are not without drawbacks. At high temperatures in oxidising environments, SiC will form a protective SiO_2 layer however in the presence of steam, as found in gas turbines, the usually protective SiO_2 will form volatile silicon hydroxide ($Si(OH)_4$), resulting in a recession of SiC [3].

Naturally, SiC-based CMCs must be protected from such environments; one approach to do this is through coating the CMC, known as an environmental barrier coating (EBC). Similar to how thermal barrier coatings have been employed to protect nickel superalloys from high temperatures, EBCs can be used to protect CMCs from steam recession. To be effective, the EBC must have; low silicon volatilisation, a coefficient of thermal expansion (CTE) similar to that of the CMC, chemical compatibility with the CMC and phase stability over the range of operating temperatures [4]. For over 30 years, silicates have been investigated for use as EBCs due to their combination of properties and the ease with which they can be deposited using thermal spray techniques, primarily atmospheric plasma spraying (APS) [5,6]. More recently, rare-earth silicates, specifically ytterbium monosilicate (Yb_2SiO_5 or YbMS) and ytterbium disilicate ($Yb_2Si_2O_7$ or YbDS), are considered state-of-the-art due to their low CTE (7.5×10^{-6} K^{-1}, measured over a

* Corresponding author.
E-mail address: Tanvir.Hussain@nottingham.ac.uk (T. Hussain).

https://doi.org/10.1016/j.ceramint.2023.04.053
Received 24 February 2023; Received in revised form 23 March 2023; Accepted 7 April 2023
Available online 8 April 2023

Table 1
YbDS APS parameters for all 11 spray runs with coating thickness.

Spray Number	Power (kW)	Current (A)	Ar (psi/ SLM)	H_2 (psi/ SLM)	Stand-off Distance (mm)	Robot Scanning Speed (mm/s)	Feedstock	Number of Passes (Thickness μm)
Effect of Spray Power								
1	**12**	400	95/85	30/2	150	610	YbDS	2 (70 ± 10)
2	**16**	300	95/85	40/3	150	610	YbDS	2 (81 ± 8)
3	**20**	400	95/85	40/3	150	610	YbDS	2 (90 ± 7)
4	**24**	500	95/85	40/3	150	610	YbDS	2 (96 ± 8)
Effect of Stand-off Distance								
5	12	400	95/85	30/2	**100**	610	YbDS	10 (322 ± 22)
6	12	400	95/85	30/2	**125**	610	YbDS	10 (313 ± 20)
7	12	400	95/85	30/2	**150**	610	YbDS	10 (247 ± 30)
Effect of PE Addition								
8	24	500	95/85	40/3	150	1000	**YbDS**	20 (350 ± 40)
9	12	400	95/85	30/2	125	1000	**YbDS**	25 (385 ± 34)
10	12	400	95/85	30/2	125	1000	**YbDS + 1.5 wt% PE**	25 (397 ± 36)
11	12	400	95/85	30/2	125	1000	**YbDS + 4.5 wt% PE**	35 (410 ± 25)

range of 473–1673 K and 4.1 × 10^{-6} K^{-1}, measured over a range of 303–1873 K respectively), excellent phase stability and the fact they present a single polymorph over the operating temperature range [7–10].

Beyond higher operating temperatures, another practical way in which the efficiency of gas turbines can be increased is to reduce leakages that occur during the compression and turbine stages. This can be achieved by reducing the clearances between the moving parts within the turbine, for example, between the blades and the casing. Due to the high operating temperatures within the turbine, the blades will expand and contact the casing if the clearance is too low, high loads and large vibrations could also lead the blade to impact the casing. To get around this, abradable seal coatings can be employed. Such coatings are soft enough to be worn away by the turbine blade tip (without damaging the tip itself), allowing for tighter clearances to be used, limiting leakages and increasing efficiency, whilst still (in the case of an abradable EBC) providing protection of the CMC substrate from steam recession. Abradable seals are typically made up of a matrix phase to which pore forming phases (e.g. polyester) and/or solid lubricants (e.g. hBN or $LaPO_4$) are added to provide abradability [11,12]. While research into abradable EBCs is still in its infancy, studies have been conducted into a hBN containing YbDS APS deposited EBCs, and within industry patents regarding polyester and solid lubricant containing EBCs have been granted [13–15].

Many studies have been undertaken regarding the optimisation of YbDS deposition [5,16–18]. In particular, Richards et al. [5] used a Praxair SG-100, a widely used plasma spray torch similar to the type used in this study, to obtain a dense YbDS coating with relatively low YbMS phase content while exploring a range of spray parameters. In order to obtain a crystalline coating the spray was conducted inside a furnace, a setup up not feasible for high volume coating production. Despite this, the requirements of an abradable coating are vastly different to that of an EBC. To prevent the ingress of steam, EBCs must provide a gas-tight seal over the CMC substrate, whereas porosity is inherent in abradable coatings. While Qin et al. [13] have investigated the wear resistance of hBN containing YbDS abradable coatings and Tejero-Martin et al. [12] have determined the resistance of abradable YbDS coatings to CMAS attack, no fundamental study has been conducted on the deposition of abradable YbDS coatings. If abradable EBCs are to be considered for the next generation of gas turbines, their deposition needs to be better understood. The aim of this study was to determine an optimum deposition condition for an abradable YbDS system maximising the level of porosity. Bearing this in mind, a parametric investigation was undertaken to optimise a YbDS coating deposited by APS. The effect of spray power and stand-off distance were investigated, the phase composition, microstructure and level of porosity were characterised for all the coatings. Finally, polyester acting as a pore former, was added to the feedstock and these coatings characterised.

2. Methodology

2.1. Materials

EBC and abradable EBC systems were deposited using APS. The coating system is comprised of a reaction bonded SiC substrate (JAI Engineers, UK), an intermediate Si bond layer and YbDS as a protective top layer. Commercially available Si (Metco 4810) and YbDS (Metco 6157) (both Oerlikon Metco AG, Switzerland) were used as feedstocks for the respective layers. The Si powder had a nominal size range of 15–75 μm and contained <1.5 wt % SiO_2 and a balance of Si. The YbDS powder had a nominal size range of 11–90 μm, contained a maximum of 5 vol % of unreacted Yb_2O_3 and YbMS. Prior to spraying, the powders were treated at 80 °C for 12 h using a box furnace (Elite Thermal Systems, UK) to remove any moisture. Finally, Metco 600NS (Oerlikon Metco AG, Switzerland), a polyester (PE) powder, was mixed with the YbDS powder at 1.5 and 4.5 wt %. The pore former was a crystalline aromatic polyester powder with a nominal size range of 45–125 μm. The mixture was homogenised using a Labram acoustic mixer (Resodyn Acoustic Mixers, USA).

Reaction bonded SiC discs with a diameter of 25 mm and thickness of 10 mm, were used as the substrates. These were grit blasted using a blast cleaner (Guyson, UK) with SiC (220 mesh) particles at a pressure of 9 bar. After grit blasting the surface roughness (R_a) of the SiC discs was found to be 3.1 ± 0.1 μm (average of 3 grit blasted discs). Following surface preparation, the substrates were sonicated in industrial methylated spirit (IMS) using a FB-505 ultrasound probe (Fischer Scientific, UK) in pulse mode (1 s pulse every 2 s) at 60% amplitude. Finally, the substrates were dried using compressed air.

2.2. Coating deposition

An SG-100 plasma spray system (Praxair Surface Technology, USA) was used to deposit the coatings. The spray gun was fitted with a 02083-175 anode, 02083-120 cathode and a 03083-112 gas injector. Ar was used as the primary gas, and H_2 was used as the secondary gas.

The Si bond coat was deposited using a spray power of 27 kW, a current of 600 A, primary gas (Ar) pressure of 85 psi (equivalent to a flow rate of 75 SLM), a secondary gas (H_2) pressure of 35 psi (2.5 SLM), a stand-off distance of 125 mm, a powder feed rate of 30 g/min and the robot speed was 1000 mm/s over 6 passes. These conditions were optimised prior to this study.

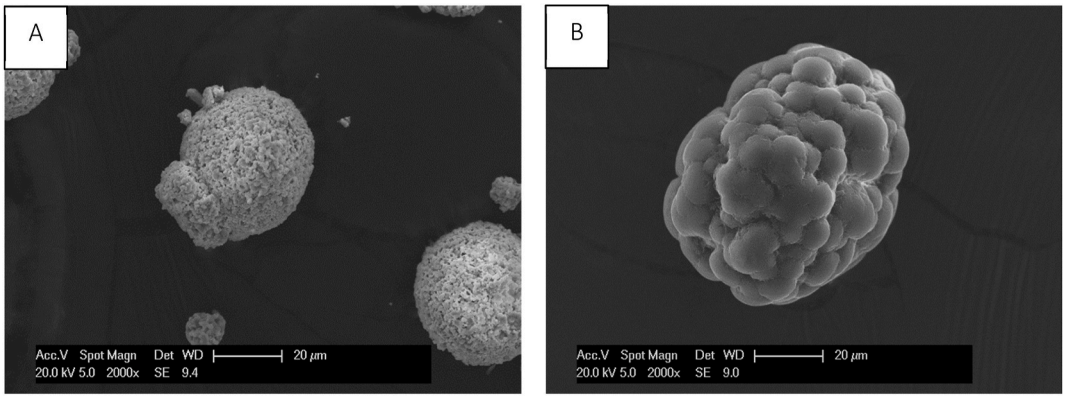

Fig. 1. SE SEM image of (a) YbDS and (b) PE powder showing sintered and agglomerated structure with some porosity.

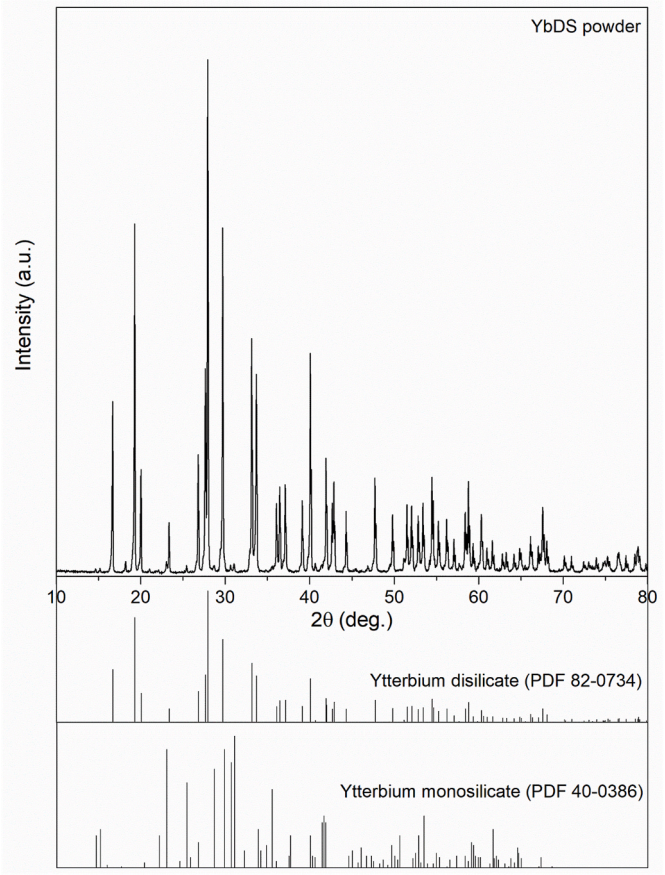

Fig. 2. Diffractogram of Metco 6157 powder showing predominantly YbDS and minor YbMS peaks.

The YbDS spraying parameters are shown in Table 1. A parametric study was conducted varying spray power to assess how this affected YbDS phase retention and porosity in the coating. To vary the spray power, arc current and secondary gas pressure were adjusted to provide four distinct power levels, 12, 16, 20 and 24 kW (sprays 1–4). Following this, a similar study was conducted with fixed spray power of 12 kW as the stand-off distance was reduced from 150 mm down to 125 and 100 mm (sprays 5–7). Coatings containing 1.5 and 4.5 wt % polyester powder mixed into the YbDS feedstock were also deposited using 12 kW spray power (sprays 10 and 11). Initially, 75–100 μm coatings were deposited to conduct basic characterisation, for sprays 8–11 a target thickness of 350–400 μm was desired for more in-depth characterisation. Initially (sprays 1–7) a robot scanning speed of 610 mm/s was used; however, when attempting to deposit thicker coatings this was found to induce deboning of the bond coat and EBC from the SiC substrate likely due to deposition rate residual stress effects, to eliminate this the robot speed was increased to 1000 mm/s in subsequent coating trials (sprays 8–11). Due to the highly amorphous nature of the as-sprayed coatings, a crystallisation heat treatment was conducted to form crystalline phases [19]. This was done at 1200 °C (Elite Thermal Systems Ltd., UK) for 2 h, with heating and cooling rates of 5 °C/min in air [12,20]. Prior to the crystallisation heat treatment, the polyester containing coatings underwent a burn-out heat treatment at 500 °C for 3.5 h with a heating rate of 5 °C/min, to burn off any remaining organic material.

The temperature and velocity of both the Si and YbDS feedstock particles were measured using a Tecnar Accuraspray 4 (Tecnar, Canada) in order to better understand the condition of the particles as they impacted the substrates. The Accuraspray has a large measurement volume of 750 mm^3 (3 mm × 25 mm x 10 mm) allowing for temperature and velocity data as an average of all of the particles passing through the measurement volume to be measured [21]. As particles pass through the focal plane of the Accurapsray system, pulses are generated by two slits in the sensor; knowing the time between the pulses and the distance between the slits the particles' velocity can be calculated. Temperature is measured using a two-colour pyrometer. The accuracy of the readings is 3% for the particle temperature measurements and 2% for the particle velocity measurements. The signal amplification factor and exposure time settings were different for the different spray parameters and stand-off distances but were comprised in the range of 20–32 times and 16–41 ms, respectively. The response time was set to 1 s. Before the data was acquired, a period of 60 s was allowed for flame stabilisation. A series of 60 measurements were acquired over a time frame of 60 s, and then averaged to give the resulting values.

2.3. Sample preparation for characterisation

Coated samples were sectioned using a Qcut 200 precision cutting machine (Metprep, UK) and abrasive diamond cut-off wheels (Metprep, UK) with a cutting speed of 0.025 mm/s. Samples in Section 3.1.1. were then hot-mounted using conducto-mount (Metprep, UK). Subsequently, the coated substrates were mounted with EpoFix resin and hardener (15:2 volumetric ratio) (Struers, Denmark) and then sectioned. The cross-sections were mounted again using EpoFix resin and hardener (Struers, Denmark). The mounted samples were then ground using a 200 grit diamond lapping disc (DK Holdings Ltd, UK). Lastly, the ground samples were polished using diamond polishing pads to a surface finish of 6 μm and 1 μm.

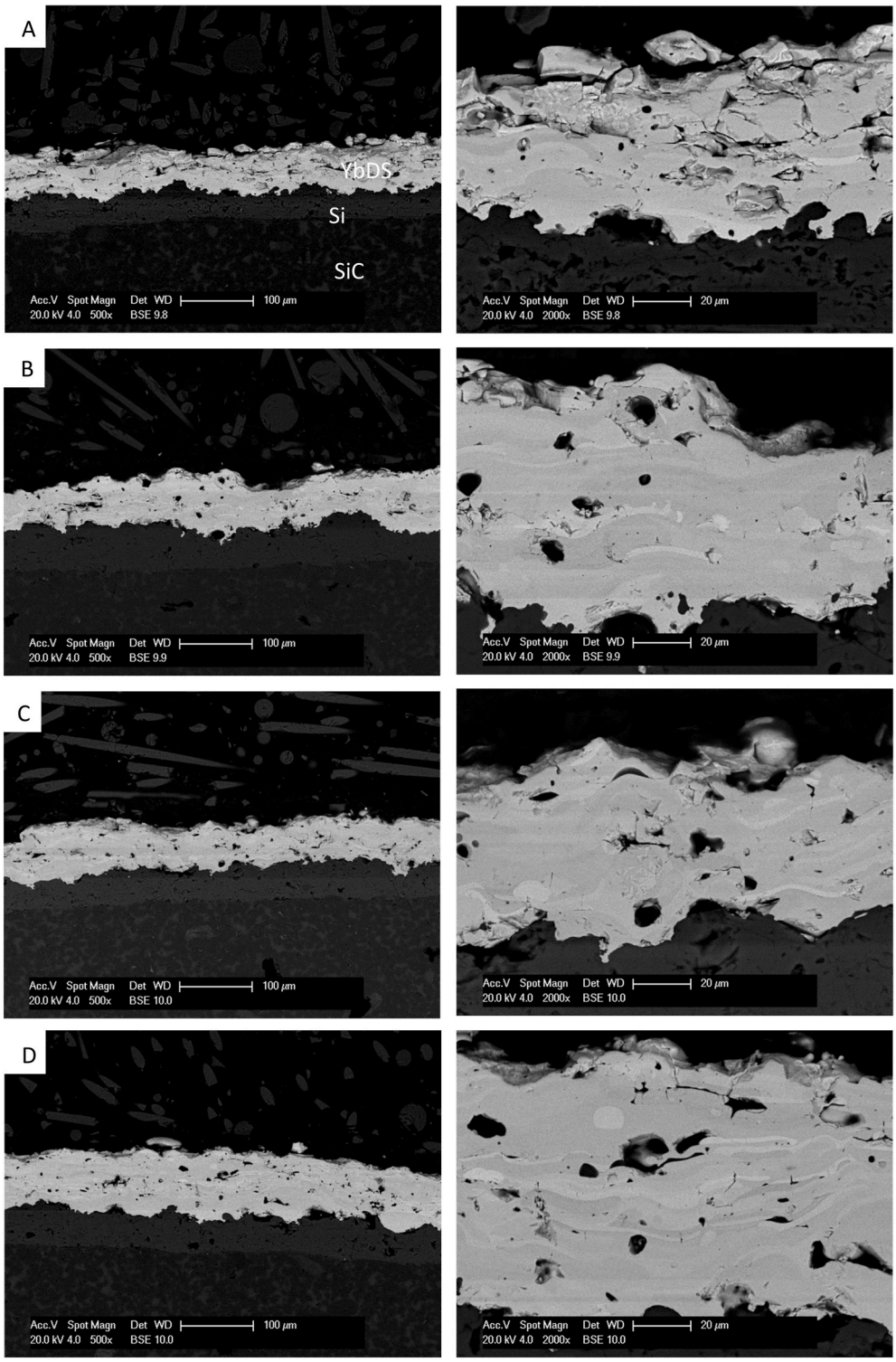

Fig. 3. BSE SEM images of heat-treated YbDS coating microstructures deposited using the four sets of spraying parameters with (a) corresponding to a spray power of 12, (b) 16, (c) 20 and (d) 24 kW.

2.4. Sample characterisation

The morphology of the YbDS powder, the microstructure of the coating and the surface topography of the coating were characterised using a FEI XL30 scanning electron microscope (SEM) (Phillips FEI, Netherlands) operated in secondary electron (SE) and backscattered electron (BSE) modes, using an accelerating voltage of 20 kV, spot size of 5 nm and working distance of ~10 mm. The SEM was equipped with energy-dispersive x-ray spectroscopy (EDX) (Oxford Instruments, UK) which was used to perform elemental analysis. The level of porosity was measured using ImageJ image processing software (National Institute of Health, USA). BSE images taken at 1000 times magnification, covering around 600 μm^2 of the cross-section, were converted into black and white maps upon setting a threshold, which was kept constant for all coatings. Then the area percentage of the image covered by porosity was measured, returning an overall value per image. An average of the

Table 2
Porosity and microhardness measurements for coatings deposited using the four spray powers.

Spray Number	Spray Power (kW)	Deposition Rate (μm/pass)	Porosity (heat-treated) (% area)	Microhardness (heat-treated) (HV0.1)	Particle Velocity (ms^{-1})	Particle Temperature (°C)
1	12	35	9.8 ± 1.1	463.4 ± 90.9	89 ± 1	1687 ± 43
2	16	41	8.3 ± 1.1	686.7 ± 77.3	100 ± 1	1889 ± 8
3	20	45	7.2 ± 0.9	718.4 ± 81.9	114 ± 1	2014 ± 11
4	24	48	5.6 ± 0.5	736.2 ± 51.5	129 ± 1	2095 ± 13

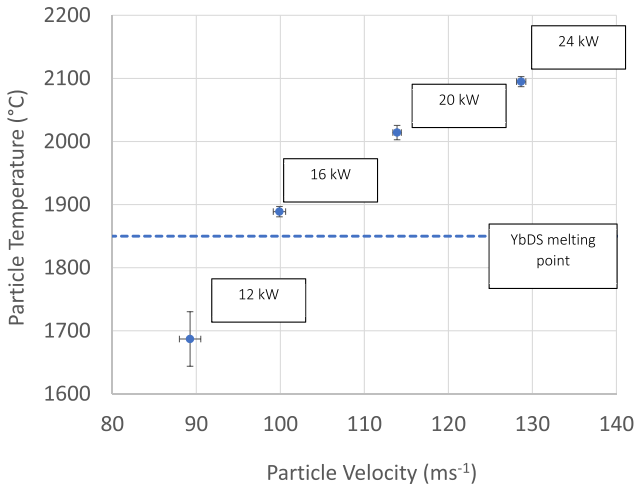

Fig. 4. A graph showing particle velocity vs particle temperature, measured with a Tecnar Accuraspray 4, for the four different spray powers.

porosity across the five images of each coating was calculated and the standard deviation was presented as the error associated with each measurement. The ImageJ measurement function was used to measure the thickness of the coatings. One measurement was taken from five BSE images taken at 250 times magnification per coating, the average and standard deviation of the five results were calculated.

Microhardness measurements were performed using a Vickers hardness indenter (Buehler, USA), an average of 5 indents was reported. A load of 100 gf was applied to the samples, testing under this load did not form cracks, and hence the only form of energy dissipation was due to the indent itself.

2.5. X-ray diffraction

The phase analysis on the feedstock powder and as-sprayed coating was conducted by XRD using a D8 Advance (Bruker, UK) from 10 to 80° 2θ, using Cu Kα radiation (0.154 nm wavelength), a 0.02° step size and 0.2 s per step using Bragg-Brentano geometry. Phase identification in the coatings was completed using EVA software (Bruker, UK) supported by data from the PDF-2 database (ICDD-PDF). Phase quantification (in wt. % according to Hill and Howard [22]) was performed using Rietveld refinement in TOPAS V5 (Bruker, UK) with reference to the guidelines outlined by McCusker et al. [23]. Rather than measuring a sample without any broadening effects, the instrumental broadening was accounted for by employing a fundamental parameters approach whereby the details of the experimental set-up (radiation source, slits, detector, etc.) are used for instrumental function calculations [24]. For all the phases observed, standard structures were taken from the Crystallography Open Database and used in the refinements.

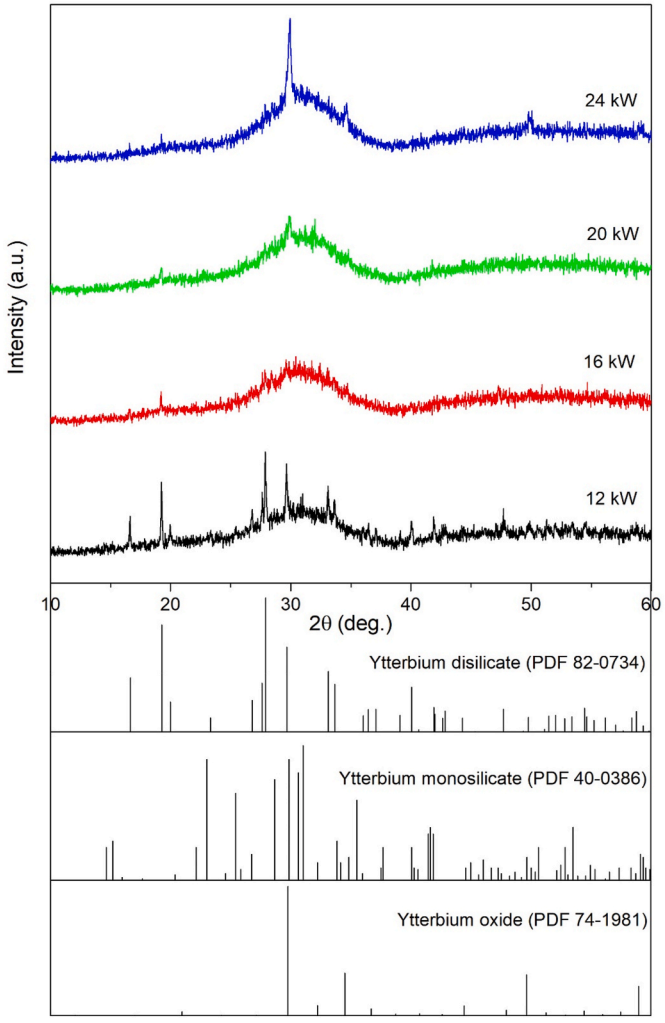

Fig. 5. XRD diffractograms for the as-sprayed coatings sprayed at 12, 16, 20 and 24 kW.

3. Results

3.1. Powder and coating characterisation

SEM analysis was carried out on the YbDS and PE powders used in this study in order to understand their morphology, micrographs of the powder particles can be seen in Fig. 1. The YbDS powder exhibits a spherical morphology with some internal pores visible from the surface, typical of agglomerated and sintered powders.

XRD of the powder is shown in Fig. 2, the composition of the powder was mainly monoclinic YbDS (*C2/m*, 82–0734) with small amounts of monoclinic YbMS (I2/a, 40–0386). The phase composition of the powder was quantified using Rietveld refinement, the powder was found to contain 95.1 wt % YbDS and 4.9 wt % YbMS.

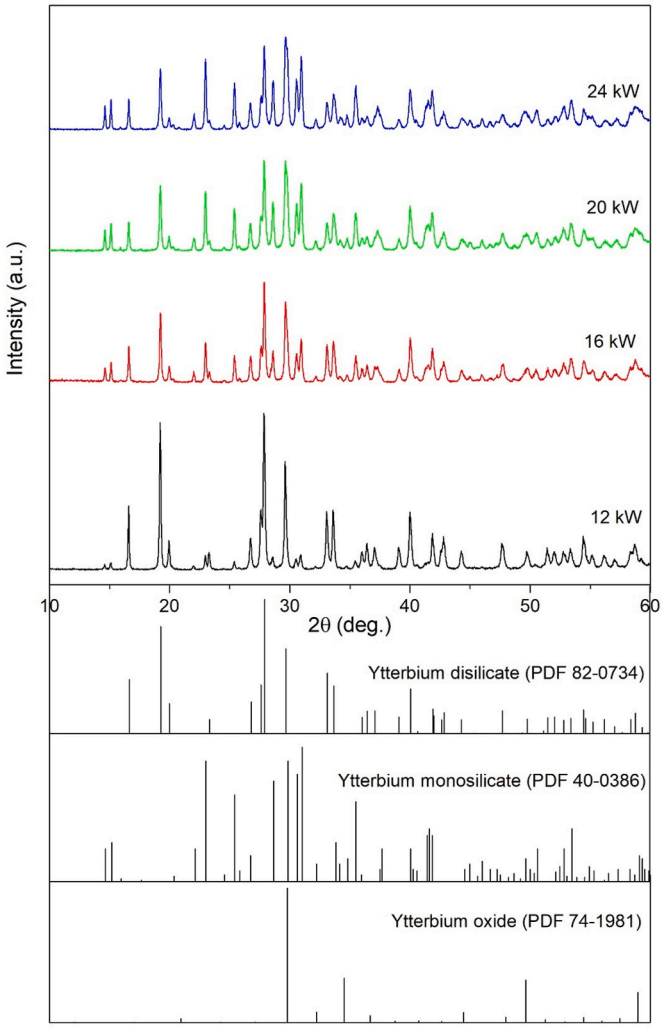

Fig. 6. XRD diffractograms of the heat-treated coatings sprayed at 12, 16, 20 and 24 kW.

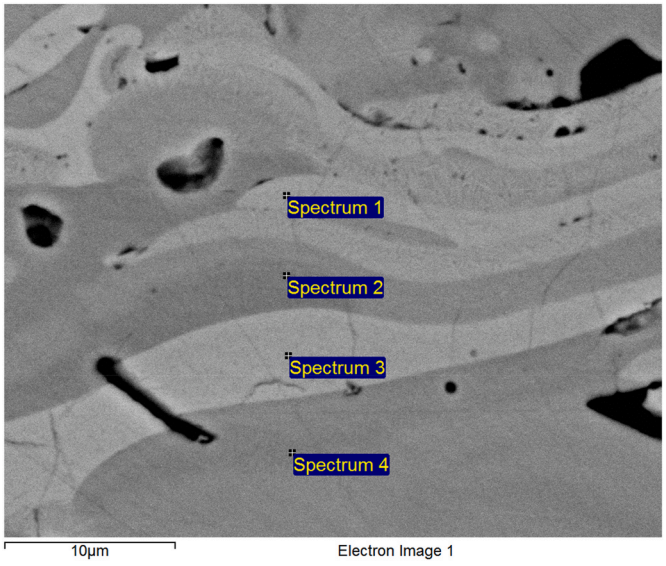

Fig. 7. A high magnification SEM image of a heat-treated YbDS coating microstructure, deposited using 24 kW parameters (spray 1). The greyscale contrast shows the presence of multiple phases.

Table 3
YbDS, YbMS and Yb2O3 content for coatings deposited using the four spray powers.

Spray Number	Spray Power (kW)	YbDS Content (wt. %)	YbMS Content (wt. %)	Yb_2O_3 Content (wt. %)
1	12	87.0 ± 0.2	13.0 ± 0.2	–
2	16	60.1 ± 0.3	39.9 ± 0.3	–
3	20	48.7 ± 0.2	51.3 ± 0.2	–
4	24	43.2 ± 0.2	52.0 ± 0.2	4.8 ± 0.1

Table 4
EDX results from the SEM image shown in Fig. 7. Spectrums 1 and 3 show EDX analysis of a brighter appearing phase while spectrums 2 and 4 show EDX analysis of a darker phase. Compared to the lighter phase the darker phase is Yb rich and Si depleted.

Element (at. %)	Yb	Si	O
Spectrum 1	27	11	62
Spectrum 2	21	16	63
Spectrum 3	27	11	62
Spectrum 4	22	15	63

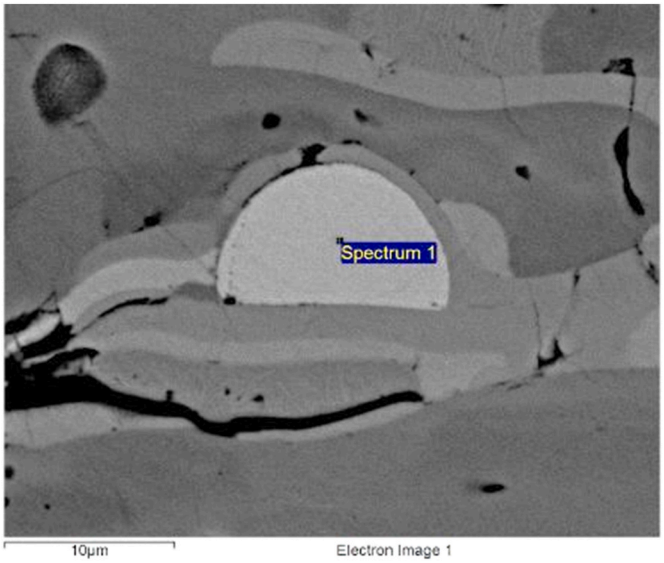

Fig. 8. EDX analysis of a suspected Yb_2O_3 particle in the coating deposited using 24 kW (spray 1) after heat treatment, spectrum 1 contained 35.1 at. % Yb, 1.2 at. % Si and 63.7 at. % O.

3.1.1. *Effect of spray power*

To investigate the effect spray power had on the phase composition and microstructure, 75–100 μm thick coatings were deposited. The spray powers used were 12, 16, 20 and 24 kW, these were selected to capture data from a broad processing window encompassing a variety of particle conditions in terms of temperature and velocity.

Fig. 3 shows BSE SEM images of the microstructures of the coatings deposited using the four spray powers after heat treatment. The coating deposited using 12 kW spray power was highly porous (~10%) after heat treatment due to the presence of partially melted and un-melted particles. The microhardness of the heat-treated coatings was measured as well as the porosity, this is shown in Table 2. Generally, porosity decreased and microhardness increased with increasing spray power in the heat-treated coatings. The deposition rate also increased with spray power, and although it wasn't measured directly and it can be inferred that the deposition efficiency would also increase, given the spray time/number of passes, powder feed rate and carrier gas flow were constant for all four of the sprays.

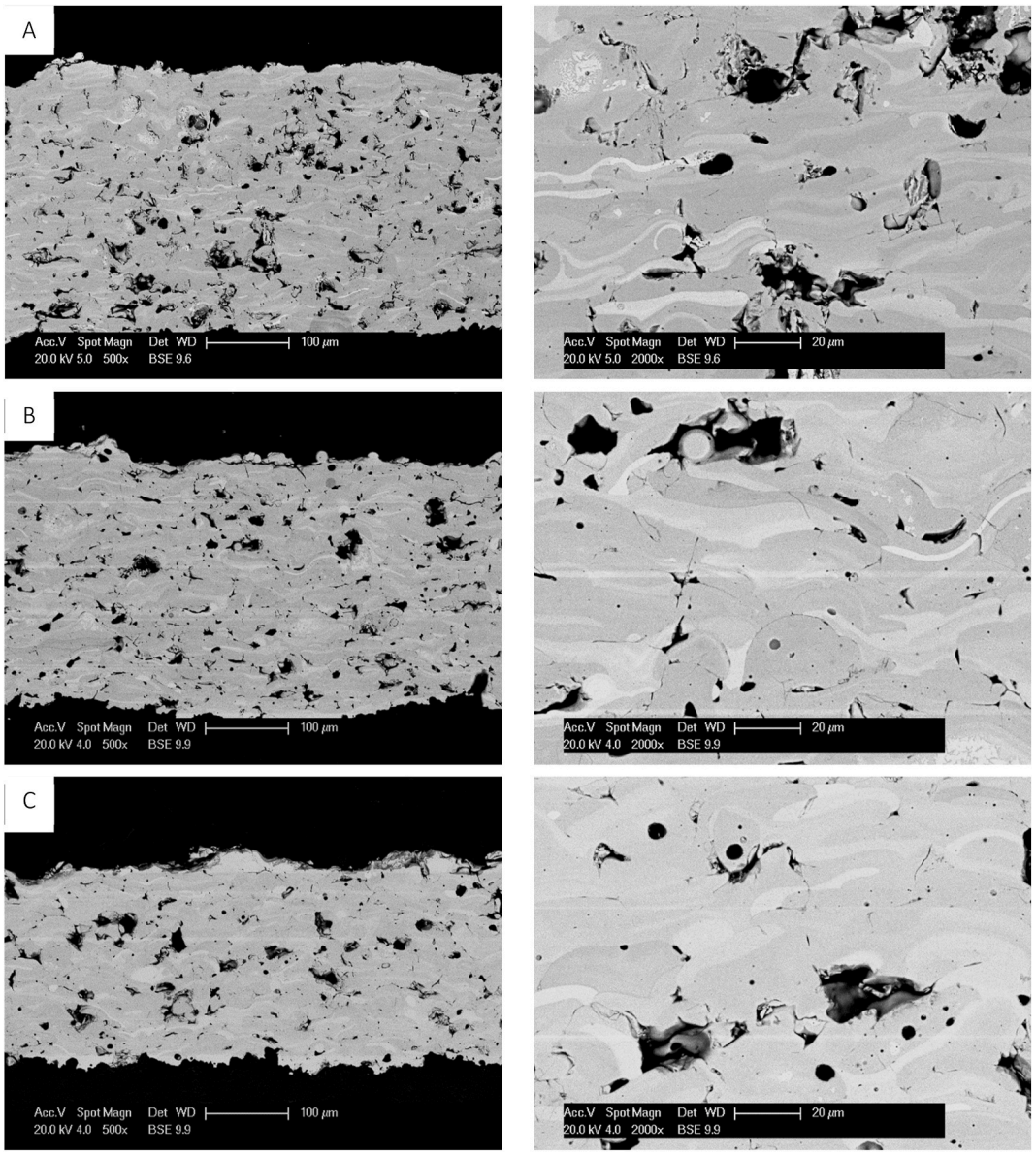

Fig. 9. BSE SEM images of heat-treated YbDS coating microstructures deposited using 12 kW spray power at various stand-off distances with (a) corresponding to a stand-off distance of 100 mm, (b) 125 and (c) 150 mm.

Table 5
Porosity, taken using ImageJ, and microhardness measurements for coatings deposited using the three stand-off distances.

Spray Number	Stand-off Distance (mm)	Deposition Rate (μm/pass)	Porosity (heat-treated) (% area)	Microhardness (HV0.1)	Particle Velocity (ms^{-1})	Particle Temperature (°C)
5	100	32	12.4 ± 0.5	735 ± 79	108 ± 1	1738 ± 17
6	125	31	10.7 ± 0.4	605 ± 113	103 ± 1	1702 ± 14
7	150	25	12.4 ± 2.4	511 ± 132	89 ± 1	1687 ± 43

The particle velocity and temperature measured at a stand-off distance of 150 mm are shown in Fig. 4, in order to understand the condition of the particles as they impacted the substrate. Both particle velocity and surface temperature increased as the spray power was increased. In this study, in order to increase the spray power, the arc current and secondary gas pressure were increased. Increasing the arc current increases the velocity and length of the plasma jet, resulting in higher particle temperatures and velocities [25]. Compared to Ar, H_2 has increased thermal conductivity and specific heat capacity leading to higher arc voltages, so the higher proportion of H_2 in the plasma gas, the more energetic the plasma [25]. Generally, higher spray powers result in a higher proportion of fully molten material (as more thermal energy is available to be transferred to the particles in the plasma), which when it impacts the substrate has the appropriate kinetic and thermal energy to form coherent, well-flattened splats, which will result in a less porous coating. The particle temperature exceeded the melting temperature of YbDS (1850 °C) [26] for all of the tested spray parameters except 12 kW, which caused a large volume of un-melted particles to be visible within the coating, causing increased porosity. While this ensures that the feedstock will be molten as it impacts the substrate, work by Richards et

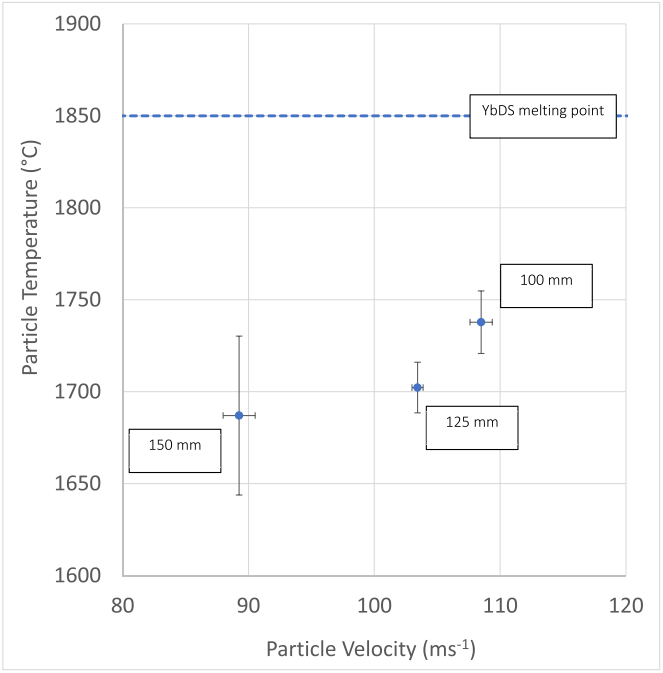

Fig. 10. A graph showing particle velocity vs. particle temperature, measured with a Tecnar Accuraspray 4, for the three different stand-off distances.

el [5]. has shown that at high temperatures (1000–3000 °C), the high vapour pressure of SiO_2 led to its depletion from the molten material, resulting in the formation of YbMS and Yb_2O_3 phases in the YbDS coating.

Increasing the spray power also had a drastic effect on the phase composition of the coatings. The heat-treated microstructures of all the YbDS coatings deposited in Fig. 3 exhibit a multi-phase structure, one appearing lighter in colour indicating it is rich in heavier elements, while the other has a darker contrast indicating a greater fraction of lighter elements. XRD analysis of the coatings in Fig. 6 identified these two phases to be YbDS and YbMS. Previous works have shown that these bands do not represent distinct equilibrium phases but, in fact, combinations of equilibrium phases, in this case, YbDS and YbMS, with the contrast coming from the proportion of each within the band [5,18].

Diffractograms of the as-sprayed and heat-treated coatings are shown in Figs. 5 and 6. The as-sprayed coatings contain mainly amorphous phases as expected in APS EBCs. Due to the high cooling rate of the particles, after they have impacted the substrate during APS, amorphous structures are formed [18,27,28]. In all of the diffractograms, two broad amorphous humps are visible between ~25° and 35° and ~40°–60°; however, some crystalline peaks can be detected in the coatings produced with 12 and 24 kW spray powers. From Fig. 5, the 12 kW coating contained peaks corresponding to monoclinic YbDS (*C*2/*m*, 82–0734), a further indication of a high volume of un-melted material. Meanwhile, in the 24 kW coating, one prominent peak can be identified at ~29°. This peak likely corresponds to cubic Yb_2O_3 ($I2_13$, 74–1981) (222), indicating excessive SiO_2 loss when using this spray power as no Yb_2O_3 was detected in the feedstock powder.

Heat treatment prompted crystallisation of the phases in the coatings, the diffractograms of the heat-treated coatings can be seen in Fig. 6. Monoclinic YbDS (*C*2/*m*, 00-082-0734) and monoclinic YbMS (I2/a, 40–0386) phases were identified in all the coatings. This two-phase structure can be seen clearly in.

Fig. 7 along with EDX analysis of the two phases shown in Table 4. EDX analysis of the phases showed the darker phases to be Si and O rich compared to the lighter phase. While the limitations of measuring oxygen with EDX due to it being a light element are understood, the atomic percentages were close to the stoichiometry of the indicated phases. Fig. 8 shows the composition of a suspected Yb_2O_3 particle in the coating deposited using 24 kW after heat treatment. The EDX analysis of the particle shows it to be almost Si free, containing only 1.2 at. % Si.

The phase composition of the heat-treated coatings was quantified by Rietveld refinement. The respective phase compositions of all the coatings are shown in Table 3. The phase composition of the coating is sensitive to the spraying parameters used in its deposition. In every coating except the one deposited using 12 kW, the amount of YbMS was greater than the amount of YbDS. Increasing the arc current and the amount of H_2 in the plasma gas composition increased the spray power, which led to increased particle temperatures, in turn leading to a higher rate of SiO_2 loss and a shift towards more Yb-rich compositions [26].

3.1.2. *Effect of stand-off distance*

While the level of porosity achieved using 12 kW spray power was desirable for an abradable coating, the microhardness of the coating was relatively low when compared to the other coatings produced. In an effort to increase the microhardness of the coatings the effect of stand-off distance was investigated while the other spray parameters remained constant. The heat-treated microstructures of the coatings deposited at 12 kW using three different stand-off distances can be seen in Fig. 9. Despite the stand-off distance being altered, the microstructures appear largely similar. All of the coatings exhibit large pores and a combination of fully, partially and un-melted particles. From Table 5, it can be seen that for all of the coatings, the level of porosity remains largely constant irrespective of the stand-off distance used in the spraying process. Despite the level of porosity remaining relatively stable the microhardness values, again shown in Table 5, increased as the stand-off distance was shortened. Increasing the stand-off distance also reduces the deposition rate and, effectively, the deposition efficiency, as explained in the previous section.

Fig. 10 shows a graph of particle velocity vs particle temperature for the three stand-off distances, measured using an Accuraspray 4. As the stand-off distance is reduced the particle velocity and temperature increase, leading to the increase in microhardness observed in the coatings. The particle temperature was still lower than the YbDS melting point when the particles impact the substrate meaning similar microstructures and levels of porosity were retained due to the presence of unmelted and partially melted particles. The particles at shorter stand-off distances impacted the substrate with higher velocities, which led to an increase in deformation of the particles, and created better-bonded splats, which in turn increased the microhardness of the coatings. Previous work on the effect plasma parameters have on coating properties has shown the relationship between reducing stand-off distance and increasing hardness [29,30]. Particularly, work by Sarikaya has shown that, when spraying alumina, by increasing stand-off distance changes in hardness can be achieved without significant changes in porosity level [29]. No difference in phase composition was detected using XRD and Rietveld refinement when the stand-off distance was changed, given all the coatings were deposited using the same spray parameters, it is likely the majority of the SiO_2 volatilisation occurred earlier in the particles' flight towards the substrate, in the highest temperature part of the plasma (<100 mm).

3.1.3. *Effect of PE addition*

Based on the work presented so far, a relatively dense YbDS EBC was deposited using 24 kW spray power at a stand-off distance of 150 mm (referred to as EBC), while a porous abradable EBC was deposited using 12 kW spray power at a stand-off distance of 125 mm (referred to as ABR). These conditions were selected to maximise the hardness of the coating and the YbDS phase. The stand-off distance of 100 mm produced highly stressed coatings with occasional delamination between the SiC substrate and the Si bond coat. To reduce this 125 mm was selected as the optimum stand-off distance while the robot scanning speed was increased to 1000 mm/s. To increase the level of porosity further, feedstocks with 1.5 wt % and 4.5 wt % PE addition to YbDS were also

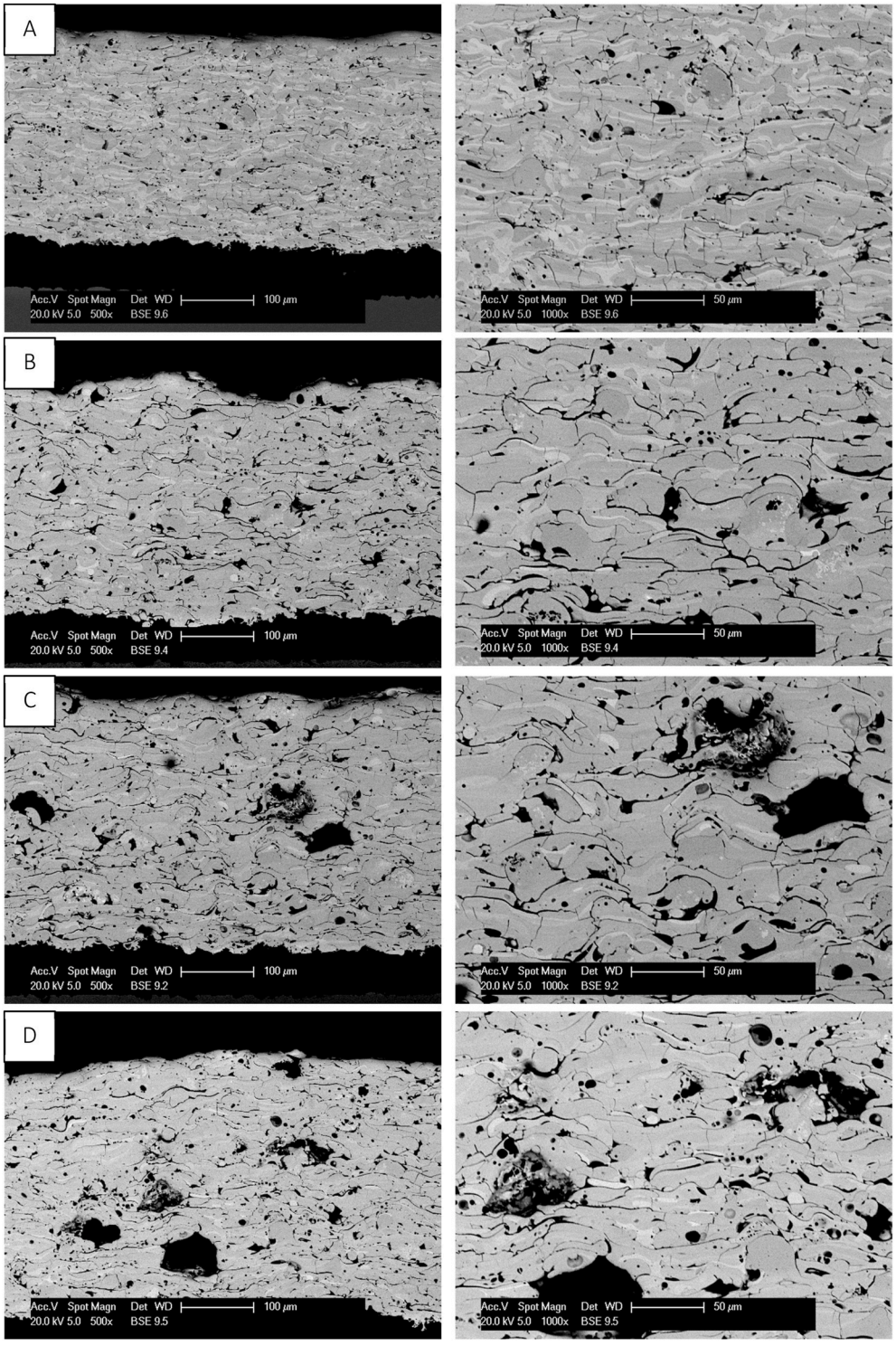

Fig. 11. BSE SEM images of as-sprayed YbDS coating microstructures deposited using various feedstocks, spray powers and stand-off distances with (a) corresponding to a relatively dense YbDS EBC deposited using 24 kW spray power at a stand-off distance of 150 mm (EBC), (b) a porous abradable YbDS EBC deposited using 12 kW spray power at a stand-off distance of 120 mm (ABR) (c) a porous abradable YbDS + 1.5 wt % PE EBC deposited using 12 kW spray power at a stand-off distance of 120 mm (ABR+ 1.5 wt % PE) and (d) a porous abradable YbDS + 4.5 wt % PE EBC deposited using 12 kW spray power at a stand-off distance of 120 mm (ABR+ 4.5 wt % PE).

deposited using 12 kW spray power (referred to as ABR + 1.5 wt % PE and ABR +4.5 wt % PE respectively). The as-sprayed microstructures of these four coatings are shown in Fig. 11, while the heat-treated microstructures are shown in Fig. 12. In its as-sprayed state, the EBC microstructure has some porosity and microcracking; however, upon heat-treatment these microcracks have healed. ABR shows a highly porous structure caused by un-melted and partially melted particles previously seen in sections 3.1.1 and 3.1.2. The addition of the PE has caused further large pores in addition to the smaller pores and inter-splat pores caused by the low spray power, as can be seen in Fig. 12c and d. The increased level of porosity caused by the addition of PE was quantified and is presented in Table 6. The porosity values for EBC and ABR are similar to what has been reported previously in sections 3.1.1 and 3.1.2; however, the addition of 1.5 and 4.5 wt % greatly increases the level of measured porosity in the coating to 14.4 and 18.9%, respectively. The addition of the PE did not cause any change in phase composition from the ABR coating, this was verified using XRD.

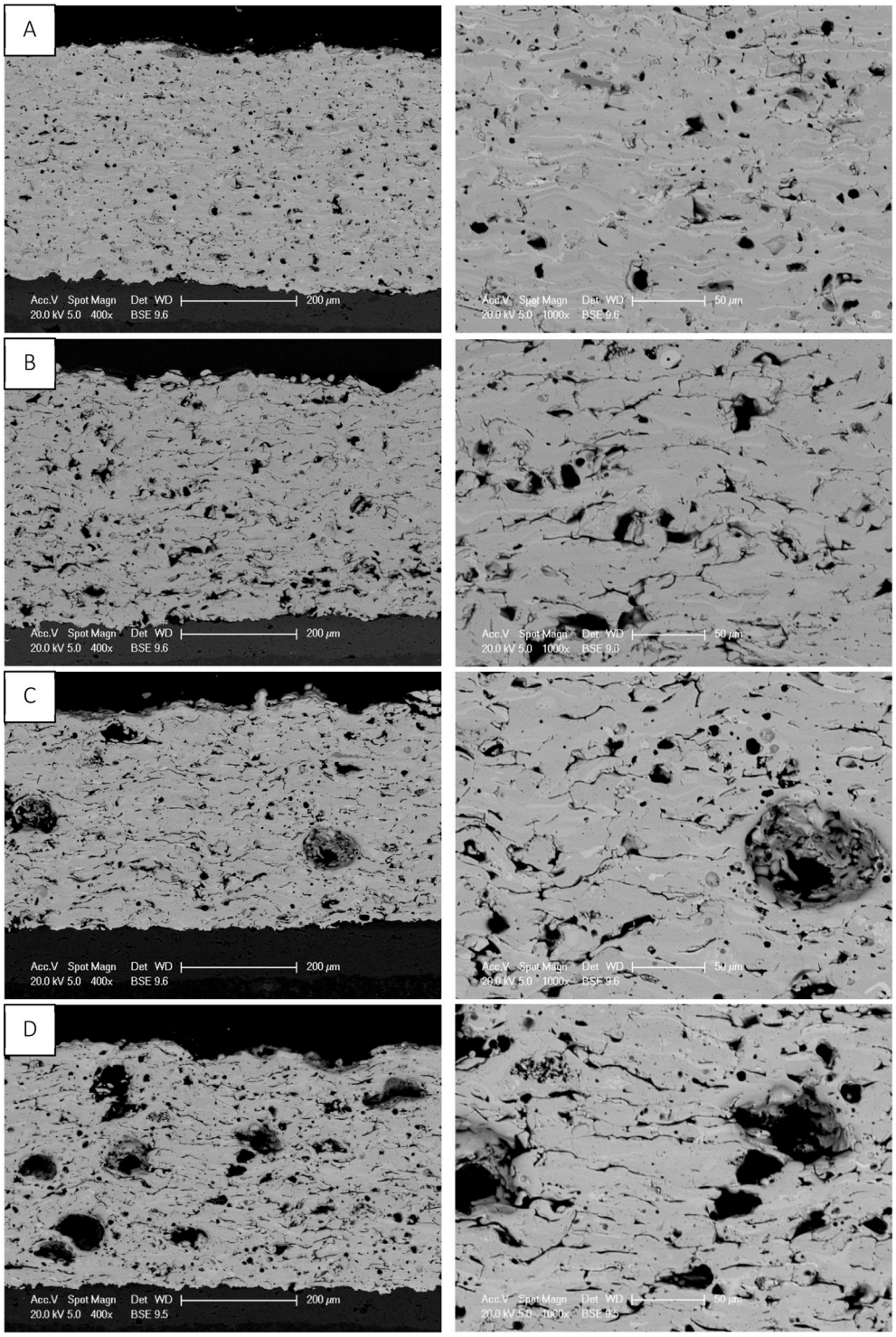

Fig. 12. BSE SEM images of heat-treated YbDS coating microstructures deposited using various feedstocks, spray powers and stand-off distances with (a) corresponding to a relatively dense YbDS EBC deposited using 24 kW spray power at a stand-off distance of 150 mm (EBC), (b) a porous abradable YbDS EBC deposited using 12 kW spray power at a stand-off distance of 120 mm (ABR) (c) a porous abradable YbDS + 1.5 wt % PE EBC deposited using 12 kW spray power at a stand-off distance of 120 mm (ABR+ 1.5 wt % PE) and (d) a porous abradable YbDS + 4.5 wt % PE EBC deposited using 12 kW spray power at a stand-off distance of 120 mm (ABR+ 4.5 wt % PE).

4. Discussion

In order to optimise the deposition process of YbDS EBCs and abradable EBCs, the effect the spray parameters and feedstock modification have on phase composition and microstructure must be understood. The coatings reported in this study present vastly different phase compositions and microstructures depending on the deposition conditions employed. During the APS process, YbDS has transformed to YbMS regardless of spray power since only a small weight percentage of YbMS was detected in the feedstock powder. Richards et al. [5] proposed this was due to the higher vapour pressure of the Si bearing species leading to its preferential volatilisation at elevated temperatures above ~1000 °C, resulting in the formation of YbMS. Between 1300 and 2500 °C the vapour pressure of the Si bearing species was $\sim 10^6$ times larger than the vapour pressure of the Yb bearing species [5]. When relating the particle temperatures measured in the plasma plume for the various spray powers in Fig. 4 to the phase quantification determined using Rietveld refinement results in Table 3; it is clear that increasing the spray power (therefore increasing the particle temperature) leads to a higher rate of SiO_2 volatilisation and a greater fraction of YbMS in the

Table 6
Porosity and microhardness measurements for the EBC and three abradable EBC coatings.

Spray Number	Coating	Porosity (Heat-treated) (% area)	Microhardness (heat treated) (HV0.1)
8	EBC	5.6 ± 0.4	783.1 ± 28.1
9	ABR	8.8 ± 0.8	695.6 ± 42.3
10	ABR + 1.5 wt % PE	14.4 ± 0.9	633.5 ± 27.6
11	ABR +4.5 wt % PE	18.9 ± 2.1	553.9 ± 50.0

coating. Increasing the spray power from 12 to 24 kW increased the average particle temperature at the point it impacted the substrate from 1687 to 2095 °C, which led to a decrease in YbDS phase content from 87 to 43 wt %. These findings are in agreement with previous studies by Chen et al. [31] and Garcia et al. [18], who also found that higher spray powers resulted in higher particle temperatures, which in turn led to increased fractions of YbMS in the respective coatings.

In the as-sprayed XRD results, one prominent peak can be identified at ~29° in the coating deposited at 24 kW. This peak likely corresponds to the plane (222) of cubic Yb_2O_3 ($I2_13$, 74–1981), indicating excessive SiO_2 loss when using this spray power as no Yb_2O_3 was detected in the feedstock powder. Yb_2O_3 has a much higher melting point than YbDS or YbMS (2355 °C, relative to 1850 °C and 1950 °C, respectively [26]), indicating the possibility of a solid crystalline phase during the spraying process, since this is below the particle temperatures measured when using this spray power (2095 °C). While previous research has not led to the discovery of Yb_2O_3 when spraying YbDS feedstocks, Richards et al. [5] did determine its presence when spraying a YbMS powder, indicating if the level of SiO_2 volatilisation is severe enough, Yb_2O_3 will form. Compared to previous studies where particle temperature and velocity have been analysed, it can be determined that the particle velocities obtained in this study were significantly lower, even when the particles temperatures were high, at higher spray powers [18,31]. This means that each particle has a longer residence time in the plasma, increasing its time at temperature and leading to a greater loss of SiO_2.

In order to form the amount of porosity required for an abradable coating, it was necessary to reduce the spray power to such an extent that some portion of the feedstock was un-melted and remained as such within the coating. This can be seen from the XRD data in Fig. 5, where crystalline YbDS peaks could still be detected in the as-sprayed 12 kW coating. If the feedstock was fully molten, it would appear as an amorphous phase rather than crystalline, as can be seen on the diffractograms of the coatings deposited at higher spray powers. While some un-melted and partially melted particles can be seen in the heat-treated microstructures in Figs. 3a and 9, a lot of the splats appear to have flattened, indicating they were at least somewhat molten as they impinged onto the substrate and formed structures typical of an APS structure. Data obtained from Accurspray 4.0 (Figs. 4 and 10) suggests that, when using 12 kW spray power, the average particle temperature is well below the melting point despite the prevalence of many fully molten splats. The averaged particle data collected using the Accuraspray system is known to be slightly weighted towards larger particles [32]; these particles will require higher thermal energy input to fully melt, hence will not reach as higher temperatures as smaller particles which are fully molten, thus skewing the particle temperature data.

While the majority of data on the level of porosity typically seen in the OEM abradable YbDS EBCs is not publicly available, abradable coatings tested by Tejero-Martin et al. [12] for CMAS recession, produced using similar equipment and feedstocks, were measured to have between 19.4 and 21.3% porosity. Previous work on other ceramic abradable coatings, specifically yttria-stabilised zirconia (YSZ) containing polyester, has typically seen porosity levels between 10 and 25% [33,34]. This suggests the abradable coatings produced in the study, as seen in Fig. 12b, c and d, are suitably porous for abradable applications provided they can provide adequate protection from steam recession and CMAS corrosion. Future work will be focused on not only this, but also how the coatings respond to abrasives in erosion testing and scaled rig testing against dummy turbine blade tips.

5. Conclusions

Abradable EBCs have the potential to greatly improve the efficiency of the latest generation of gas turbines that utilise SiC CMC components. In this work, for the first time, a parametric study was undertaken to understand how spray parameters affected the phase composition and microstructure, with the aim of creating a porous abradable coating with a commercially available and widely utilised SG-100 APS torch. By carefully adjusting the spray power and stand-off distance, the level of porosity, phase composition and microhardness was controlled. An abradable coating with ~10% porosity, ~80 wt % YbDS phase composition and ~700 HV microhardness was deposited by reducing the spray power to such a level where the particle temperature was below the melting temperature of YbDS. Subsequently, a PE pore forming phase was added to the feedstock to increase the porosity further. The addition of 1.5 and 4.5 wt % PE resulted in porosity increasing to ~14 and ~19%, respectively. Relationships between spray parameters and coating properties have also been determined. Low spray powers resulting low particle temperatures and velocities produced more porous coatings yet retained greater proportions of YbDS phase. While high spray powers producing higher particle temperatures and velocities produced harder coatings with less porosity but also less YbDS phase. The high spray powers in this study produced coatings with exceptionally high amounts of YbMS relative to previous literature. It is postulated that this is due to the high spray powers producing high particle temperatures but still relatively low particle temperatures when compared to other plasma spray systems, causing excessive time at high temperature for the particles in the plasma.

Declaration of competing interest

The authors declare that they have no known competing financial interests or personal relationships that could have appeared to influence the work reported in this paper.

Acknowledgements

This work was supported by the Engineering and Physical Sciences Research Council (EPSRC) (grant number EP/V010093/1). The project also received funding from Rolls Royce Plc in terms of a CASE PhD studentship. The authors also acknowledge the use of facilities at the Nanoscale and Microscale Research Centre of the University of Nottingham, supported by the Engineering and Physical Sciences Research Council (grant number EP/L022494/1).

References

[1] N.P. Padture, Advanced structural ceramics in aerospace propulsion, Nat. Mater. 15 (8) (2016) 804–809.
[2] J. DiCarlo, et al., SiC/SiC composites for 1200 C and above, in: Handbook of Ceramic Composites, Springer, 2005, pp. 77–98.
[3] E.J. Opila, Oxidation and volatilization of silica formers in water vapor, J. Am. Ceram. Soc. 86 (8) (2003) 1238–1248.
[4] K.N. Lee, Current status of environmental barrier coatings for Si-Based ceramics, Surf. Coating. Technol. 133–134 (2000) 1–7.
[5] B.T. Richards, H. Zhao, H.N.G. Wadley, Structure, composition, and defect control during plasma spray deposition of ytterbium silicate coatings, J. Mater. Sci. 50 (24) (2015) 7939–7957.
[6] E. Garcia, et al., Characterization of Yb2Si2O7–Yb2SiO5 composite environmental barrier coatings resultant from in situ plasma spray processing, Ceram. Int. 46 (13) (2020) 21328–21335.
[7] K.N. Lee, D.S. Fox, N.P. Bansal, Rare earth silicate environmental barrier coatings for SiC/SiC composites and Si3N4 ceramics, J. Eur. Ceram. Soc. 25 (10) (2005) 1705–1715.

[8] A.J. Fernández-Carrión, M. Allix, A.I. Becerro, Thermal expansion of rare-earth pyrosilicates, J. Am. Ceram. Soc. 96 (7) (2013) 2298–2305.
[9] B.-K. Jang, et al., Mechanical properties and microstructure of Yb2SiO5 environmental barrier coatings under isothermal heat treatment, J. Eur. Ceram. Soc. 40 (7) (2020) 2667–2673.
[10] B.T. Richards, H.N.G. Wadley, Plasma spray deposition of tri-layer environmental barrier coatings, J. Eur. Ceram. Soc. 34 (12) (2014) 3069–3083.
[11] R. Rajendran, Gas turbine coatings – an overview, Eng. Fail. Anal. 26 (2012) 355–369.
[12] D. Tejero-Martin, et al., Interaction of CMAS on thermal sprayed ytterbium disilicate environmental barrier coatings: a story of porosity, Ceram. Int. (2021).
[13] D. Qin, et al., Fabrication and characterization of Yb2Si2O7-based composites as novel abradable sealing coatings, Ceram. Int. (2021).
[14] J. Shi, L. Li, T. Freeman, Abradable Coatings for High-Performance Systems, Rolls-Royce North American Technologies, USA, 2019.
[15] R. Jackson, Environmental Barrier Multi-phase Abradable Coating, United Technologies Corporation, USA, 2020.
[16] E. Bakan, et al., Effect of processing on high-velocity water vapor recession behavior of Yb-silicate environmental barrier coatings, J. Eur. Ceram. Soc. 39 (4) (2019) 1507–1513.
[17] E. Bakan, et al., Yb2Si2O7 environmental barrier coatings deposited by various thermal spray techniques: a preliminary comparative study, J. Therm. Spray Technol. 26 (6) (2017) 1011–1024.
[18] E. Garcia, H. Lee, S. Sampath, Phase and microstructure evolution in plasma sprayed Yb2Si2O7 coatings, J. Eur. Ceram. Soc. 39 (4) (2019) 1477–1486.
[19] E. Garcia, et al., Crystallization behavior of air-plasma-sprayed ytterbium-silicate-based environmental barrier coatings, J. Eur. Ceram. Soc. 41 (6) (2021) 3696–3705.
[20] D. Tejero-Martin, et al., Steam degradation of ytterbium disilicate environmental barrier coatings: effect of composition, microstructure and temperature, J. Therm. Spray Technol. (2022).
[21] P. Fauchais, M. Vardelle, Sensors in spray processes, J. Therm. Spray Technol. 19 (4) (2010) 668–694.
[22] R. Hill, C. Howard, Quantitative phase analysis from neutron powder diffraction data using the Rietveld method, J. Appl. Crystallogr. 20 (6) (1987) 467–474.
[23] L. McCusker, et al., Rietveld refinement guidelines, J. Appl. Crystallogr. 32 (1) (1999) 36–50.
[24] P. Scardi, M. Leoni, R. Delhez, Line broadening analysis using integral breadth methods: a critical review, J. Appl. Crystallogr. 37 (3) (2004) 381–390.
[25] M. Vardelle, A. Vardelle, P. Fauchais, Spray parameters and particle behavior relationships during plasma spraying, J. Therm. Spray Technol. 2 (1) (1993) 79–91.
[26] J. Felsche, The crystal chemistry of the rare-earth silicates, in: Rare Earths, Springer Berlin Heidelberg, Berlin, Heidelberg, 1973.
[27] N. Rohbeck, P. Morrell, P. Xiao, Degradation of ytterbium disilicate environmental barrier coatings in high temperature steam atmosphere, J. Eur. Ceram. Soc. 39 (10) (2019) 3153–3163.
[28] R. Vaßen, et al., Environmental barrier coatings made by different thermal spray technologies, Coatings 9 (12) (2019) 784.
[29] O. Sarikaya, Effect of some parameters on microstructure and hardness of alumina coatings prepared by the air plasma spraying process, Surf. Coating. Technol. 190 (2) (2005) 388–393.
[30] D. Thirumalaikumarasamy, K.S. Kamalamoorthy, V.B. Visvalingam, Effect of experimental parameters on the micro hardness of plasma sprayed alumina coatings on AZ31B magnesium alloy, J. Magnesium Alloys 3 (3) (2015) 237–246.
[31] D. Chen, et al., In-flight particle states and coating properties of air plasma sprayed ytterbium disilicates, Surf. Coating. Technol. 417 (2021), 127186.
[32] S. Chadha, R. Jefferson-Loveday, T. Hussain, Modelling Knudsen number effects in suspension high velocity oxy fuel thermal spray, Int. J. Heat Mass Tran. 152 (2020), 119454.
[33] D. Aussavy, et al., YSZ-polyester abradable coatings manufactured by APS, J. Therm. Spray Technol. 25 (1–2) (2016) 252–263.
[34] Y. Cui, et al., Evolution of the residual stress in porous ceramic abradable coatings under thermal exposure, Surf. Coating. Technol. 394 (2020), 125915.